X-ray spectroscopy of super-intense laser-produced plasmas for the study of nonlinear processes. Comparison with PIC simulations

E Dalimier[1], A Ya Faenov[2,3], E Oks[4], P Angelo[1], T A Pikuz[3,5], Y Fukuda[6], A Andreev[7,8], J Koga[6], H Sakaki[6], H Kotaki[6], A Pirozhkov[6], Y Hayashi[6], I Yu Skobelev[3,9], S A Pikuz[3,9], T Kawachi[6], M Kando[6], K Kondo[6], A Zhidkov[5], E Tubman[10], N M H Butler[11], R J Dance[11], M A Alkhimova[3,9], N Booth[12], J Green[12], C Gregory[12], P McKenna[11], N Woolsey[10] , R Kodama[2,5]

[1] LULI - UPMC Paris 06 : Sorbonne Universités ; CNRS, Ecole Polytechnique, CEA : Université Paris-Saclay - F-75252 Paris cedex 05, France
[2] Institute for Academic Initiatives, Osaka University, Suita, Osaka, 565-0871, Japan
[3] Joint Institute for High Temperatures, Russian Academy of Sciences, Moscow 125412, Russia
[4] Physics Department, 206 Allison Lab, Auburn University, Auburn, AL 36849, USA
[5] PPC and Graduate School of Engineering, Osaka University, 2-1, Yamadaoka, Suita, Osaka 565-0871, Japan
[6] Kansai Photon Science Institute, National Institutes for Quantum and Radiological Science and Technology, Kizugawa, Kyoto, 619-0215, Japan
[7] Max Born Institute, Berlin 12489, Max-Born str.2a, Berlin, Germany
[8] ELI-ALPS, Szeged H-6720, Hungary
[9] National Research Nuclear University MEPhI (Moscow Engineering Physics Institute), Moscow 115409, Russia
[10] York Plasma Institute, Department of Physics, University of York, York YO10 5DD, UK
[11] Department of Physics, SUPA, University of Strathclyde, Glasgow G4 0NG, UK
[12] Central Laser Facility, STFC Rutherford Appleton Laboratory, Didcot OX11 0QX, UK

E-mail: elisabeth.dalimier@upmc.fr

Abstract. We present X-ray spectroscopic diagnostics in femto-second laser-driven experiments revealing nonlinear phenomena caused by the strong coupling of the laser radiation with the created plasma. Among those nonlinear phenomena, we found the signatures of the Two Plasmon Decay (TPD) instability in a laser-driven CO_2 cluster-based plasma by analyzing the Langmuir dips in the profile of the O VIII Lyε line, caused by the Langmuir waves created at the high laser intensity 3 10^{18}Wcm^{-2}. With similar laser intensities, we reveal also the nonlinear phenomenon of the Second Harmonic Generation (SHG) of the laser frequency by analyzing the nonlinear phenomenon of satellites of Lyman δ and ε lines of Ar XVII. In the case of relativistic laser-plasma interaction we discovered the Parametric Decay Instability (PDI)-induced ion acoustic turbulence produced simultaneously with Langmuir waves via irradiation of thin Si foils by laser intensities of 10^{21}Wcm^{-2}.

1. Introduction

X-ray spectroscopy in femto-second laser-driven plasmas can be used for a better understanding of intense laser-plasma interaction. Undoubtedly it can also be used for a laboratory modelling of nonlinear physical processes in astrophysical objects. The nonlinear phenomena caused by the strong coupling of the electromagnetic wave "t_1" of the laser at frequency ω_L (and eventually its second

harmonic "t_2" at $2\omega_L$) with the created plasma may involve the Langmuir turbulence "l" at the electron plasma frequency ω_{pe} equal to ω_L (or $\omega_L/2$) and the ion acoustic turbulence "s" at the ion plasma frequency ω_{pi}. The processes discovered in the present work, due to high-resolution X-ray spectroscopy, are the Two Plasmon Decay instability TPD [1], the Parametric Decay Instability PDI and the Second Harmonic Generation SHG [2]. For TPD the nonlinear process is summarized by the balance equation $t_1 \rightarrow l + l$. For PDI the process involved is $t_1 \rightarrow l + s$ and as for SHG it can be explained either by the process $l+l \rightarrow t_2$ or $l + t_1 \rightarrow t_2$.

The two super intense femto-second laser facilities involved in these spectroscopic studies of non-linear processes are the Kansai Photon Science Institute (KPSI, National Institutes for Quantum and Radiological Science and Technology, Kyoto, Japan) and the Rutherford Appleton Laboratory RAL (Science and Technology Facilities Council, Didcot, UK).

At KPSI, the lasers JLITE-X (pulse duration 40 fs, pulse energy 60 mJ) and J-KAREN (pulse duration 40 fs, pulse energy 800 mJ) gave access to large intensities $4\ 10^{17}$ Wcm^{-2} and $3\ 10^{18}$ Wcm^{-2} respectively. As for the Vulcan Petawatt laser (pulse duration 500-1500 fs, pulse energy 290 J), relativistic laser-plasma regimes could be reached with intensities as high as $1.4\ 10^{21}$ Wcm^{-2}.

2. Discovery of the Two Plasmon Decay TPD instability

At KPSI, the spectroscopic analysis of the Langmuir dips of O VIII Lyε line revealed the instability process TPD and its characteristics [1].

Let us first recall the mechanism of Langmuir dips formation adding some improvements in their spectral line shape characteristics. The L-dip phenomenon is a resonant coupling between the low frequency ionic field F_i and the quasi-monochromatic electric field E of the high frequency Langmuir wave ω_{pe}. The resonance condition is given by:

$$\omega_F = s\omega_{pe}(N_e) \qquad (1)$$

where $\omega_F = 3n\hbar F_i/(2Z_r m_e e)$ is the separation between Stark sublevels caused by F_i (n being the principal quantum number and Z_r the nuclear charge of radiating ion) and $\omega_{pe} = (4\pi e^2 N_e/m_e)^{1/2}$, the electron plasma frequency (N_e being the electron density). s=1 for "one quantum" resonance.

Due to the broad distribution ΔF of the low frequency field, there is always a fraction of radiators, for which the resonance condition is satisfied.

The resonance condition manifests as an L-dip (for each Stark component) located from the unperturbed wavelength $\lambda_{0,}$ at the distance $\Delta\lambda_{dip}$ given in equation (2) (see, e.g., [3]):

$$\Delta\lambda_{\delta\iota\pi} = -[\lambda_0^2/(2\pi\chi)]\{\theta\omega_{\pi\varepsilon} + [2\omega_{\pi\varepsilon}^3/(27\nu^3 Z_\rho Z_\pi \omega_{\alpha\tau})]^{1/2}[\nu^2(\nu^2 - 6\theta^2 - 1) + 12\nu^2\theta^2 \pm 6\nu^2\theta]\} \qquad (2)$$

The positions of the dips allow an accurate measure of the electronic density N_e as they depend on it as:

$$\Delta\lambda_{dip} = aN_e^{1/2} + bN_e^{3/4} \qquad (3)$$

Here a and b are controlled by quantum numbers n and q and by the charges of the radiating Z_r and perturbing Z_p ions (n is the principal quantum-number, $q = n_1 - n_2$ the electric quantum number, n_1, n_2 being the parabolic quantum-numbers). $\omega_{\alpha\tau} = 4{,}14\ 10^{16}\ \sigma^{-1}$ is the atomic unit of frequency. The first term in equation (3) is due to the dipole interaction with the micro-field and the second to the quadrupole interaction.

Figure 1 shows the two bump-dip-bump structures in O VIII Lyε line that lead to a spectroscopic diagnostic of TPD. These structures are the one quantum resonance (s=1) dip in the profiles of the two most intense components, originating from the sublevels (311) and (131), (q=2 and q=-2 the electric quantum number values). By comparing the theoretical and experimental separations between these two L-dips

$$[\lambda_0^2/(\pi c)]|q|\rceil_{pe}(N_e) = 4(\lambda_0^2/2\pi c)\rceil_{pe}(N_e) = 4\lambda_p = 57\text{mA} \quad (4)$$

we determine ω_{pe}= 1.26 x 10^{15} s^{-1}= ω_{pe} and then find that it is equal to $\omega_L/2$ with the accuracy 5%.

Since the TPD instability occurs at the quarter of the critical density $N_c=m_e\omega_L^2/4\pi e^2$, the above constitutes the experimental evidence of the TPD. It is important to emphasize that the center of gravity of the structures is shifted to the red by 9 mA, in agreement to the non-uniformity of the ion micro-field effect [4] reflected by the second term in the right side of Eq. (2).

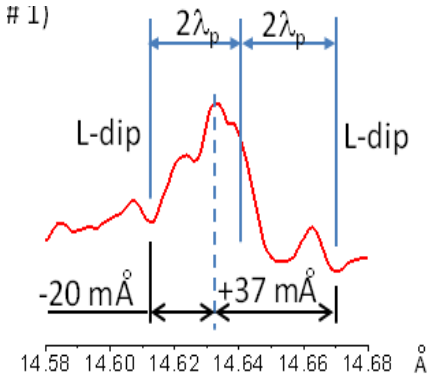

Figure 1. The two "bump-dip-bump" structures in O VIII Lyε line . The experiment was performed at J-Karen in femto-second laser-driven cluster- based experiments with mixture CO_2 and He (laser frequency ω_L= 2.4 10^{15} s^{-1}, laser intensity I_L = 3 10^{18} Wcm^{-2}). The bumps surrounding the dips are due to partial transfer of the intensity from the wavelength of the dip to adjacent wavelengths.

3. Discovery of the PDI induced ion acoustic turbulence

At RAL, at the relativistic laser intensities, the spectroscopic analysis of the Langmuir dips in Si XIV lines and of the excessive ("anomalous") Stark broadening of these lines, led to the conclusion of the development of Low-frequency Electrostatic Turbulence (LET) caused by the PDI. Using Vulcan petawatt laser facility (wavelength λ_L= 1.045 μm; pulse duration 500 to 1500 fs; intensity I_L up to 1.4 10^{21} Wcm^{-2}), the ultra-intense radiation penetrates the plasma until a region of density N_{rc} higher than the usual critical density N_c [5]. The density N_{rc} is higher than N_c because of the relativistic increase of the mass of electrons, and thus the decrease of the electron plasma frequency.

For the linearly - polarized laser radiation, the relativistic critical density is given by [6]

$$N_{rc} = (\pi a/4)\, N_c \quad (5)$$

with $N_c(\omega) = m_e\omega_L^2/(4\pi e^2)$ and $a = \lambda_L(\mu m)\,[I_L(\omega/cm^2)/(1.37x10^{18})]^{1/2}$

For the Vulcan laser the critical density N_c can be 1.0 10^{21} cm^{-3} and in consequence the relative critical density could be as high as N_{rc}= 2.3 10^{22} cm^{-3}. In fact it is well known that in relativistic regimes the transverse electromagnetic wave intensity is higher than the incident laser radiation intensity due to self-focusing of the beam, Raman and Brillouin backscattering [7], so that the relativistic critical density should be even higher, as we will confirm.

Figure 2 shows typical X-ray spectra of Si XIV Lyβ and Lyγ lines at Vulcan with two laser irradiations of silicon foils. The black trace is for the incident laser radiation 1.01 10^{21} Wcm^{-2} at the surface of the target, the blue trace for a laser irradiation 0.24 10^{21} Wcm^{-2}.

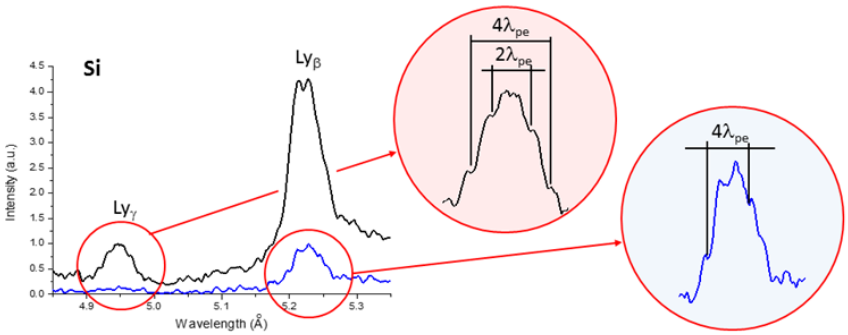

Figure 2. Observation of the Langmuir dips in Lyβ (blue trace) and Lyγ (black trace) corresponding to different incident laser irradiations 0.24 10^{21} Wcm^{-2} (blue trace) and 1.01 10^{21} Wcm^{-2} (black trace).

The identification of the symmetrical L-dips on Lyβ (blue trace) separated by 43mA yields (with s=1 and q=±2) the density N_e=1.74 10^{22} cm^{-3}. The identification of the two couples of symmetrical dips on Lyγ (with s=1, q=±1 for the dips separated by 28mA, and with s=1, q=±2 for the dips separated by 56mA) yields the same density N_e=3.6 10^{22} cm^{-3}.

If the low-frequency (quasistatic) field involved in the formation of L-dips would be represented by the ion microfield, there would be a significant red shift of the center of gravity of all those pairs of L-dips in Fig. 2 (according to the second term in the right side of Eq. (2). However, the experimental profiles do not show any such red shift. This is the experimental evidence that the low-frequency (quasistatic) field involved in the formation of L-dips was dominated by the LET (in which case there is no second term in Eq. (2)).

This is the first (but not the only one) confirmation that the LET was developed at the surface of relative critical density N_{rc}. It is well-known that at this surface the mechanism for the production of the LET is the PDI, i.e., the transformation of the laser wave into the combination of the Langmuir wave and the ion acoustic wave. The density N_{rc} for each shot (blue and black traces) is higher than the density given by (5), as predicted.

There is a second confirmation that the low frequency field is dominated by LET developing at N_{rc}. This confirmation comes from line broadening analysis. Line broadening simulations have been made and compared with two kinds of simulations: the FLYCHK modelling [8] and the Oks's modelling. FLYCHK code takes into consideration the Stark broadening with the ionic micro field and the Doppler, opacity and instrumental broadenings. This code is valid even for high densities $10^{23}cm^{-3}$. In this simulation the Langmuir dips and the LET broadening are excluded. The Oks's modeling valid only for moderate densities has the advantage to take into account the Langmuir dips, and the Stark broadening with both the ionic field and the LET. It takes into consideration the Döppler, opacity and instrumental broadenings, just as FLYCHK.

Figure 3 shows for Si XIV Lyγ the FLYCHK simulation fitting with the experimental result obtained at RAL. The electronic density for the fit is 9 $10^{22}cm^{-3}$ which is obviously higher than 3.6 $10^{22}cm^{-3}$, the density measured from the dips separations and identified to the relativistic critical density. Figure 4 presents Oks' simulation for the same line Si XIV Lyγ. The electron density for the good fit is 3.6 $10^{22}cm^{-3}$, exactly the measured density for the relativistic critical density. Obviously this simulation supports the presence of the LET, i.e. the ion acoustic wave, in the relativistic plasmas.

A third confirmation of the presence of the LET accompanying the PDI in relativistic regimes was obtained by PIC simulations shown in figure 5. 1D PIC simulation for a laser pulse duration 600 fs with intensity 2.7 10^{21} Wcm^{-2} (the estimated intensity of the transverse electromagnetic wave) has been performed. The initial scaled density of Si ions was taken constant over 2μm on the foil. The black line corresponds to the transverse electric field, the blue line to the longitudinal Langmuir wave. The red and green lines represent the evolutions of the electron and ion densities respectively. The

Langmuir wave exists up to N_{rc}= 3.6 10^{22}cm^{-3}. The modulation of the ion density is the manifestation of the ion acoustic wave.

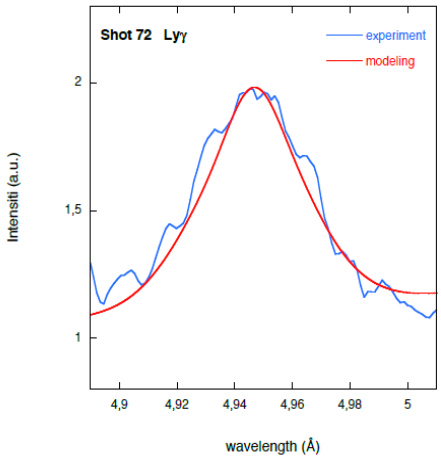

Figure 3. Si Lyγ spectral line shape with FLYCHK (red line) fitted with the experimental results (blue line)

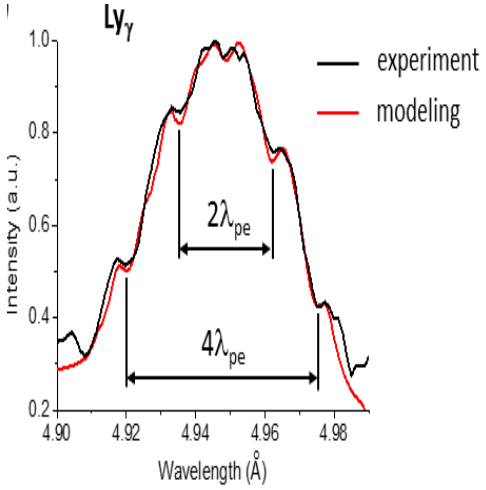

Figure 4. Si Lyγ spectral line shape with Oks's simulation (red line) fitted with the experimental results (black line)

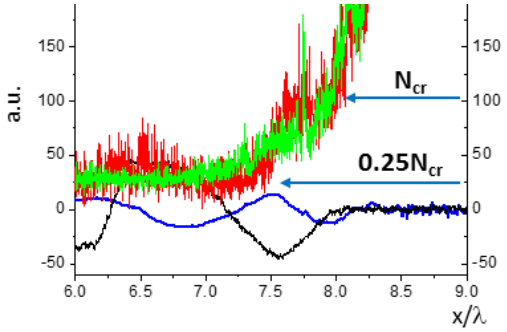

Figure 5. 1D PIC simulation of the PDI in the relativistic regime showing the modulation of the ion density near N_{rc}. Black line: transverse electric field. Blue line: longitudinal Langmuir wave. Red line: electron density. Green line: ion density

4. Discovery of the Second Harmonic Generation SHG of the laser frequency.

At J-KAREN facility, the Second Harmonic Generation SHG was discovered by analyzing the nonlinear phenomenon of satellites on the spectral lines Ar XVII Heδ and Heε. The intensity of the laser is high but not relativistic. In the presence of the laser electromagnetic field ω_L, the combined system "radiator plus laser field" is characterized by quasi-energy levels separated by $\hbar\omega_L$ leading in spectra to satellites $\pm\omega_L$, $\pm2\omega_L$, … Due to the high laser intensity various nonlinear processes can occur: for instance the parametric decay instability PDI can be followed by the processes l+l → t_2 or l + t_1 → t_2 . In the present work we discovered the satellites $\pm2\omega_L$, $\pm4\omega_L$, … of the transverse wave t_2 at $2\omega_L$. At J-Karen the femto second laser-driven cluster-based argon plasma was diagnosed due to a high spectral resolution (3000) and spatial resolution FSSR spectrograph. Figure 6 presents the experimental profiles (dashed blue lines) Heδ and Heε at I_L= 3 10^{18} Wcm^{-2}. The lines exhibit satellites at $2\omega(\lambda_n^2/(2pc))$, λ_n being the unperturbed wavelength, but not at $\omega(\lambda_n^2/(2\pi c))$.

Two important remarks lead to the necessity to develop a new theory of laser satellites under the action of a bi-chromatic field ω and 2ω. First, the second harmonic wave t_2 intensity being much lower

than the pump wave t_l intensity, the satellites at ω_L should be stronger than those at $2\omega_L$. This is not the case in the experiment. Moreover the second harmonic is supposed to penetrate the plasma until the density $4N_c$=7.2 10^{21} cm^{-3} (N_c being the critical density for ω_L), but the average density deduced from the spectra is lower. As a consequence a new theory had to be developed improving Blochinzev's [9] and Oks's [10, 3] theories of satellites valid only for the lateral Stark components of hydrogen lines under a monochromatic field. Let us remark that the highly excited lines Heδ,ε are hydrogenic for the densities considered. The line Heε has a central Stark component, so that the theory of satellites was advanced by extending it to the central Stark components. Also a further advance was made by developing a theory of satellites in a bi-chromatic field $E_1\cos(\omega t) + E_2\cos(2\omega t)$ in the plasma region diagnosed by spectroscopy.

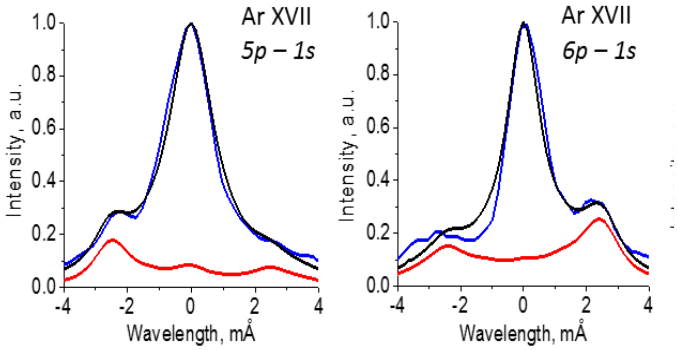

Figure 6. Ar XVII Heδ and ε profiles obtained at J-KAREN at I_L= 3 10^{18} Wcm^{-2}. The blue lines are for the experimental profiles, the solid red lines for the theoretical profiles from a bi-chromatic region and the solid black lines for the total theoretical profiles including a region of no-periodic-field. The black lines exhibit satellites at $2\omega_L$.

The argon Heδ and ε profiles obtained at J-KAREN at I_L= 3 10^{18} Wcm^{-2} are shown in figure 6.

The best agreement of the experimental profiles was obtained with simulations (solid black lines) involving a space integration over a bi-chromatic field region at the electronic density 3 10^{20} cm^{-3} (solid red lines), explaining the broad pedestals of the final profiles, and a no-periodic field region at the electronic density 10^{20} cm^{-3} reproducing the intense central part of the profiles. The simulations confirm the laser satellites at $2\omega_L$. The intensity of the SHG in the plasma versus the incident laser field in vacuum has been evaluated at 2% from the above spectroscopic analysis.

It is important to emphasize that at lower laser intensity 4 10^{17} Wcm^{-2} (JLITE-X laser at KPSI) the Second Harmonic Generation was not detected.

Finally 2D PIC simulations to support SHG diagnostics yielded fruitful results. They were performed for a 40 fs pulse of 3 10^{18} W cm^{-2} linearly polarized laser on to Ar XVII cluster 500 nm diameter. The figure 7 (a) gives the 2D spatial distribution of electric field $E_y(y,z)$ at 42 fs (z-axis laser pulse propagation from bottom to the top, cluster center at z=y=10 mm); the transformation of the plane waves into spherical waves is obvious. The distribution of the electric field along the z-axis is given in figure 7 (b) confirming the conversion efficiency into $2\omega_L$: 2%.

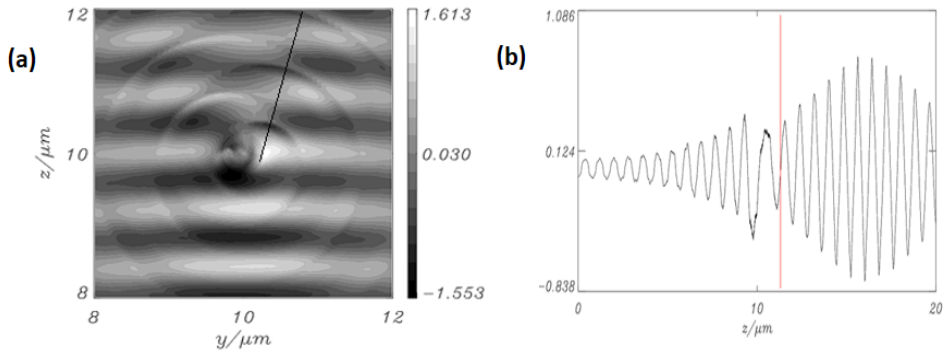

Figure 7. 2D PIC simulations for the experimental conditions, taking care of all non-linear processes for SHG (non restricted to parametric processes). (a) the 2D spatial distribution of the electric field $E_y(y,z)$; (b) the distribution of the electric field along the z-axis.

5. Conclusion

We demonstrated that X-ray spectroscopy in femto-second laser plasmas leads to a better understanding of nonlinear physical processes, such as TPD, PDI, SHG, in these plasmas. No less important is that it can be also used in a laboratory modelling of nonlinear physical processes in astrophysical objects because in both situations the ratio of the energy density of the turbulent field to the thermal energy density is of the same order. This non-perturbing method opens up an avenue for diagnosing these processes, measuring their thresholds and testing theories. The nonlinear process responsible of the PDI has been totally identified by X-ray spectroscopic diagnostic. The PIC simulations supported the discovery of the ion acoustic turbulence and the conversion of the short, intense laser light into the second harmonic generation.

Acknowledgments

We thank the Vulcan (CRL, UK) and J-KAREN and JLITE-X (KPSI, Japan) technical preparation teams for their support during the experiments. The research leading to these results has received funding from the Science and Technology Facilities Council, and the Engineering and Physical Science Research Council (Grant No.EP/J003832/1) of the United Kingdom. This work was partly supported by the Funding Program for Next Generation World-Leading Researchers (NEXT Program) from JSPS, a Grant-in-Aid for Scientific Research (A) No. 26247100 by JSPS, and the Consortium for Photon Science and Technology (CPhoST) program by MEXT. The work is partly supported by Russian Foundation for Basic Research via grants #15-32-21121 and #14-22-02089 and RAS Presidium Program for Basic Research #13. A.A. gratefully acknowledges the computing time granted by NIC and provided on the supercomputer JUROPA at JSC.

References

[1] Oks E, Dalimier E, Faenov A Ya et al. 2014 *J. Phys. B: At. Mol. Opt. Phys. Fast Track Communications* **47** 221001
[2] Oks E, Dalimier E, Faenov A Ya et al. 2015 *Optics Express* **23** 31991
[3] Oks E 1995 *Plasma Spectroscopy: The Influence of Microwave and Laser Fields* (*Springer Series on Atoms and Plasmas)* vol 9 (Berlin Springer)
[4] Oks E, Bödeeker S and Kunze H-J 1991 *Phys. Rev.* A **44** 8338
[5] Lünow W 1968 *Plasma Phys.* **44** 879
[6] Guerin S, Mora P, Adam JC, Laval G 1996 *Phys. Plasmas* **3** 2693
[7] Pukhov A 2003 *Rep. Prog. Phys.* **66** 47, Mourou GA, Tajima T, Bulanov SV 2006 *Rev. Modern Phys.* **78** 309, Sauvan P et al. 2009 *J. Phys. B: At. Mol. Opt. Phys.* **42** 195501
[8] Chung HK, Chen MH, Morgan WL, Ralchenko Yu, Lee RW 2005 *High Energy Density Physics* **1** 3
[9] Blochinzew D I 1933 *Phys. Z. Sow. Union* **4** 501
[10] Oks E 1984 *Sov. Phys. Doklady* **29** 224